Likelihood Map Waveform Tracking Performance for GNSS-R Ocean Altimetry

Santiago Ozafrain, Pedro A. Roncagliolo, and Carlos H. Muravchik

***Abstract*—Ocean altimetry with Global Navigation Satellite Systems signals (GNSS) signals is a remote sensing technique that measures the height of the sea surface through the difference in path length of the direct and reflected signal. Code altimetry estimates this parameter by tracking the code delay after performing correlations with a GNSS signal replica. It is of limited precision due to the low signal-to-noise ratio (SNR) and narrow bandwidth of the ocean-reflected GNSS signal. However, the potential advantages of the GNSS-R systems such as high temporal resolution and spatial coverage are a motivation to improve its altimetric precision. In this article, we present a performance assessment of the Likelihood Map Waveform tracking technique, a method based on Maximum Likelihood Estimation theory that exploits the available reflected power in a more efficient way than the single tracking point methods. We use a modification of the theoretical optimal solution that achieves a better performance than previous methods. We estimate it, in terms of SNR gain, using Monte Carlo method with a detailed stochastic model of the signal, and with actual signals from the Cyclone Global Navigation Satellite System. The gain values obtained were between 1.64 and 3.66 dB in the theoretical analysis, and between 1.69 and 2.62 dB with the real data, confirming the potential of the proposed approach.**

***Index Terms*—GNSS+R, Low Earth Orbit (LEO), maximum likelihood estimation, ocean altimetry, remote sensing.**

I. Introduction

REFLECTOMETRY with Global Navigation Satellite Systems signals (GNSS-R) has enabled many new Earth observation techniques. Ocean altimetry is one of them and its objective is to measure the sea surface height by estimating the difference between the path length of the reflected and direct signal captured by a receiver on the ground, airborne, or spaceborne.

Manuscript received July 31, 2019; revised November 14, 2019 and December 12, 2019; accepted December 16, 2019. Date of publication January 16, 2020; date of current version February 4, 2020. This work was supported by ANPCyT PICT 2017-0857 and UNLP 11-I-209 and CIC-PBA. Part of the work was carried on while Santiago Ozafrain visited the University of Colorado Boulder Ann and H. J. Smead Department of Aerospace Engineering Sciences funded by Fulbright Comission and Ministerio de Educación de La Nación Argentina. *(Corresponding author: Santiago Ozafrain.)*

S. Ozafrain and P. A. Roncagliolo are with the Sistemas Electrónicos de Navegación y Telecomunicaciones, Facultad de Ingeniería, Universidad Nacional de La Plata, B1900 La Plata, Argentina (e-mail: santiago.ozafrain@ing.unlp.edu.ar; agustinr@ing.unlp.edu.ar).

C. H. Muravchik is with the Instituto de Investigaciones en Electrónica, Control y Procesamiento de Señales (LEICI; UNLP-CONICET) and CIC-PBA, B1900, La Plata, Argentina (e-mail: carlosm@ing.unlp.edu.ar).

Digital Object Identifier 10.1109/JSTARS.2019.2963559

The GNSS-R signal processing typically involves the calculation of the delay-Doppler map (DDM) obtained by cross correlating the reflected signal and a local replica for a range of code delay and Doppler shift values, performing coherent short integrations, and followed by a noncoherent averaging of those results. In this article, we focus on the processing of ocean-reflected GNSS signals received on board LEO satellites, where the DDM presents a spread distribution of the correlation power in the delay-Doppler plane due to the diffuse reflection process. Its shape and power distribution depends on the bistatic radar geometry and the roughness of the ocean surface, generally resembling a horseshoe. The difference in the path length between direct and reflected signal is measured by tracking the delay value of the specular reflection point (SP) through certain observables of the DDM or its Correlation Waveform (WF), i.e., the values corresponding to the Doppler bin of its maximum value. There are multiple methods for tracking the reflected signal, Mashburn *et al.* [1]–[3] presented performance comparisons between the most common methods using real signals from both the Technology Demonstration Satellite-1 (TDS-1, [4]) and Cyclone Global Navigation Satellite System (CYGNSS, [5]) missions. The single tracking point approach that achieves the best performance according to [1] is the so-called HALF method, later renamed p70, that consists of tracking the delay value corresponding to the 70% of the WF maximum value. In [1], it is shown that the quality of the altimetric measurement depends heavily on the signal-to-noise ratio (SNR) of the DDM/WF. Since the reflected signal is very weak, it is necessary to use high-gain antenna arrays to capture it and averaging during long integration times. Naturally, in comparison with monostatic radar remote sensing systems designed for altimetry, GNSS-R is outperformed in terms of precision, mainly because of its low transmitted power and limited bandwidth. On the other hand, the GNSS-R sensors are passive, lighter, and more economic than active monostatic radar systems since they consist of modified GNSS receivers. This enables the feasibility of GNSS-R satellite constellations that achieve high temporal resolution and spatial coverage.

The fact that the signal power is spread in the delay-Doppler plane suggests that the algorithms, which are based only in observables of the WF do not exploit the signal's resources as efficiently as using the complete DDM would. In [6], we presented the derivation of the Maximum Likelihood Estimator (MLE) of the SP delay based on a signal model that takes into account the delay and Doppler spread of the reflected signal. This

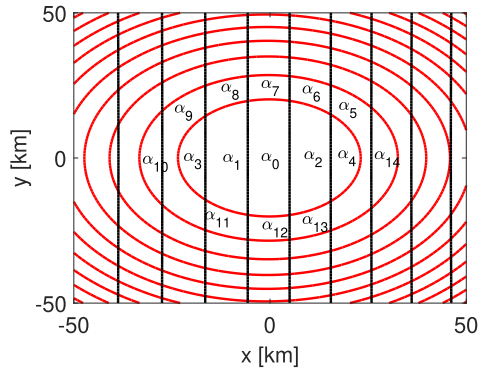

Fig. 1. Isodelay and iso-Doppler curves with 1 chip and 500-Hz separation.

estimator consists of tracking the maximum of a map analogous to the DDM, which we named Likelihood Map (LM), and is generated by processing the intermediate frequency (IF) signal, making it a so-called preprocessing method.

Even though the LM approach is optimal in the MLE sense, it does not seem to be suitable for the case of ocean-reflected signals captured by a spaceborne receiver due to its extremely weak SNR. In this article, we analyze a modified version of this algorithm designated as modified LM (MLM) that avoids the difficulties that faces the optimal solution. Moreover, this modification uses the already averaged DDM values for the calculation of each point in the map, making MLM a post-processing approach in contrast to the theoretically optimal method. In order to characterize its performance, we followed a Monte Carlo approach using the Zavorotny and Voronovich (ZV) model [7] along with a complete statistical characterization to generate DDM realizations and calculated the precision in the estimation obtained with the MLM in comparison with the p70 scheme. In addition, we applied the proposed method to a dataset of actual DDMs from CYGNSS and verified the improvement in precision using the MLM with real data.

The rest of this article is organized as follows. Section II describes the signal model used in this article and the representation of the DDM following it, along with a brief introduction to code-based ocean altimetry. Section III presents the derivation of the LM method that we proposed, its limitations, and the modified version MLM. In Section IV, we present the statistical model for the DDM that we use in the simulations and the results obtained, both with synthetic and CYGNSS DDMs. Section V concludes this article.

II. Ocean-Reflected Signal Model and Altimetry

The signal model used in this article is based on the discretization of the glistening zone into a nonuniform grid, as depicted in Fig. 1, given by the iso-Doppler and iso-delay lines projected over the ocean surface, in a similar way as [8]. Then, the reflected signal captured by a spaceborne receiver can be modeled as a linear combination of multiple returns or contributions arriving to the antenna from the center of each cell within the grid. We call model size M to the number of significant contributions that make up the total reflected signal and use the subscript m to refer to each individual return. These are characterized by their delay-Doppler pair (τ_m, f_m) defined by the position of their corresponding cell relative to the SP, and a complex amplitude α_m that models their magnitude and phase.

Considering K consecutive batches of N samples using a sampling rate $f_s = 1/T$, the received signal is described by

$$x^k[n] = \sum_{m=0}^{M-1} \alpha_m^k c(nT - \tau_m - \tau_{sp}; f_m + f_{sp}) + v^k[n] \quad (1)$$

where the superscript k indicates that the values corresponds to the kth signal segment taking values from 0 to $K-1$, (τ_{sp}, f_{sp}) is the delay-Doppler pair of the SP, $v[n]$ models the thermal noise as a complex Gaussian process with zero mean and variance σ_v^2 and $c(nT, f)$ is the GNSS signal composed of the pseudorandom signal $a(nT)$ and the carrier at frequency f: $c(nT, f) = a(nT)e^{j2\pi f nT}$.

For a more convenient representation, we use a vector form of the signal model through the following definitions:

$$\boldsymbol{\alpha}^k = \begin{bmatrix} \alpha_0^k \\ \vdots \\ \alpha_{M-1}^k \end{bmatrix}; \quad (2)$$

$$\mathbf{v}^k = \begin{bmatrix} v^k[0] \\ \vdots \\ v^k[N-1] \end{bmatrix}; \quad (3)$$

$$\mathbf{c}_m(\tau, f) = \begin{bmatrix} c(-\tau - \tau_m; f + f_m) \\ c(T - \tau - \tau_m; f + f_m) \\ \vdots \\ c((N-1)T - \tau - \tau_m; f + f_m) \end{bmatrix}; \quad (4)$$

$$\mathbf{C}(\tau, f) = \begin{bmatrix} \mathbf{c}_0(\tau, f) & \mathbf{c}_1(\tau, f) \dots \mathbf{c}_{M-1}(\tau, f) \end{bmatrix}. \quad (5)$$

Hence, the signal model becomes

$$\mathbf{x}^k = \begin{bmatrix} x^k[0] \\ \vdots \\ x^k[N-1] \end{bmatrix} = \mathbf{C}_{sp}\boldsymbol{\alpha}^k + \mathbf{v}^k, \quad k = 0 \dots K-1 \quad (6)$$

where

$$\mathbf{C}_{sp} = \mathbf{C}(\tau_{sp}, f_{sp}). \quad (7)$$

A. Delay Doppler Map

As stated previously, the usual approach to process the reflected signal in spaceborne scenarios consists of performing cross correlations with a local replica of the GNSS signals for a range of code delay and Doppler deviation values. This is a similar procedure to the GNSS signal acquisition and, after the noncoherent average of several complex cross-correlation

results, it generates the DDM that represents the correlation power distribution in the delay-Doppler plane.

Following the signal model described in the previous section, the cross-correlation result for a given delay-Doppler pair (τ, f) is obtained with the following expression:

$$y^k(\tau, f) = \frac{1}{\sqrt{N}} \sum_{n=0}^{N-1} x^k[n] c^*(nT - \tau; f). \tag{8}$$

Then, the DDM generated through the noncoherent average of (8)

$$Z_{\text{DDM}}(\tau, f) = \frac{1}{K} \sum_{k=0}^{K-1} |y^k(\tau, f)|^2. \tag{9}$$

The function $Z_{\text{DDM}}(\tau, f)$ represents the correlation power for each pair (τ, f) in the delay-Doppler plane.

B. Code Altimetry With DDM

Many GNSS-R techniques use observables obtained from the DDM, for example, its SNR and volume are related to the roughness of the ocean surface and the speed of the wind affecting it [9], also in recent studies regarding land sensing, it has been demonstrated that the SNR is related to the water content in the reflecting surface enabling soil moisture retrieval from space [10]. In ocean altimetry, the objective is to estimate the height of the sea surface through the difference in the direct and reflected signal path length. Usually, the coherent component of the reflected signal is very weak due to the diffuse reflection over the rough ocean surface, making the carrier phase tracking not practical in those cases. Therefore, the code altimetry techniques use the delay of the code signal relative to the direct one, which can be estimated from the DDM itself or its WF. The phase of the signal carrier can also be used to perform altimetry measurements achieving higher precision than code altimetry. The signal must have a strong coherent component in order to do so, which only happens in special conditions [11].

There are many available algorithms to perform the code delay estimation. The most straightforward is MAX, following the notation in [1], which consists of tracking the delay corresponding to the maximum of the WF. It would be a good solution if the reflecting surface was flat; however, it presents poor precision and is biased when applied to the scattered GNSS signal over the ocean surface. The DER method outperforms MAX in terms of precision by tracking the maximum of the derivative of the WF and gives a closer estimate to the SP delay value in diffuse reflections. The single-tracking point that presents the best performance according to [1] is p70, which is a modification of the MAX that tracks the 70% of the WF maximum value. Fig. 2 depicts a WF generated with the ZV model and synthetic noise, and the MAX and p70 tracking points. In Section IV, we compare MLM to the results obtained with p70, that is the single tracking point method with the best precision, according to [1].

III. LM Waveform

In order to formally derive an estimator for the SP code delay value, we followed the MLE theory applied to the model

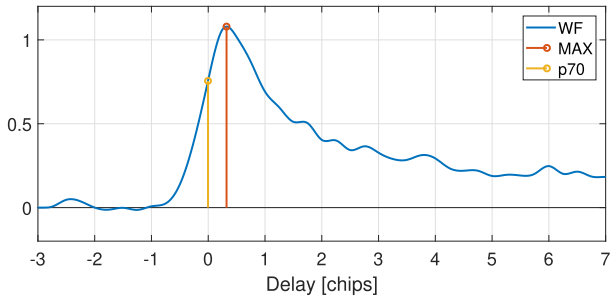

Fig. 2. DDM Waveform and tracking points.

presented in Section II. According to that representation, the joint probability density of N signal samples is

$$p(\mathbf{x}^k) = \frac{1}{\pi\sigma_v^2} \mathrm{e}^{-\frac{1}{\sigma_v^2}(\mathbf{x}^k - \mathbf{C}_{sp}\boldsymbol{\alpha}^k)^{\mathrm{H}}(\mathbf{x}^k - \mathbf{C}_{sp}\boldsymbol{\alpha}^k)}. \tag{10}$$

We consider that the set of M delay-Doppler pairs defining the signal model $(\{\tau_m, f_m\}_{m=0\ldots M-1})$ is known, since the iso-delay and iso-Doppler curves can be obtained with the geometry information and an appropriate Earth model. On the other hand, the SP delay-Doppler pair (τ_{sp}, f_{sp}) is considered unknown as well as the set of complex amplitudes that models the magnitude and phase of each contribution in the kth signal segment, represented in the vector $\boldsymbol{\alpha}^k$ as defined in (2).

We derived their MLEs $\hat{\boldsymbol{\alpha}}^k$, $\hat{\tau}_{sp}$ and $\hat{f}_{sp}$ by maximizing the Likelihood Function (LF, $l(\boldsymbol{\alpha}^k, \tau_{sp}, f_{sp})$), that is, the probability density in (10) interpreted as a function of the unknown parameters. As detailed in [6], the MLE for the set of complex amplitudes is

$$\hat{\boldsymbol{\alpha}}^k = \frac{1}{\sqrt{N}} \boldsymbol{\chi}^{-1} \mathbf{y}^k(\tau, f)|_{(\tau,f)=(\hat{\tau}_{sp}, \hat{f}_{sp})} \tag{11}$$

where

$$\boldsymbol{\chi} = \frac{1}{N} \mathbf{C}^{\mathrm{H}}(\tau, f) \mathbf{C}(\tau, f) \tag{12}$$

is the deterministic correlation matrix of the contributions that make up the signal. Its elements correspond to the Woodward Ambiguity Function (WAF), and it does not depend on (τ, f). Also, $\mathbf{y}^k(\tau, f)$ is a vector, whose elements are the complex cross-correlation results, as defined in (8), using a set of replicas with the delay-Doppler values $\{\tau_m, f_m\}_{m=0\ldots M-1}$ relative to the pair (τ, f),

$$\mathbf{y}^k(\tau, f) = \frac{\mathbf{C}^{\mathrm{H}}(\tau, f)\mathbf{x}^k}{\sqrt{N}} = \begin{bmatrix} y^k(\tau + \tau_0, f + f_0) \\ \vdots \\ y^k(\tau + \tau_{M-1}, f + f_{M-1}) \end{bmatrix}. \tag{13}$$

Then, we obtain the MLEs $(\hat{\tau}_{sp}, \hat{f}_{sp})$ by replacing the expression in (11) in the LF and maximizing it, yielding

$$l(\hat{\boldsymbol{\alpha}}^k, \hat{\tau}_{sp}, \hat{f}_{sp}) = \max_{\tau, f} (\mathbf{y}^k(\tau, f))^{\mathrm{H}} \boldsymbol{\chi}^{-1} \mathbf{y}^k(\tau, f). \tag{14}$$

Hence, the solution is to perform a 2-D maximum search for the expression above.

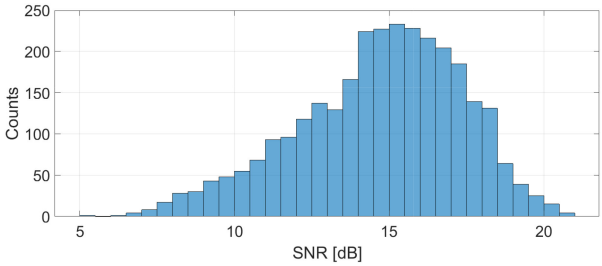

Fig. 3. Histogram of the SNR values observed in the dataset.

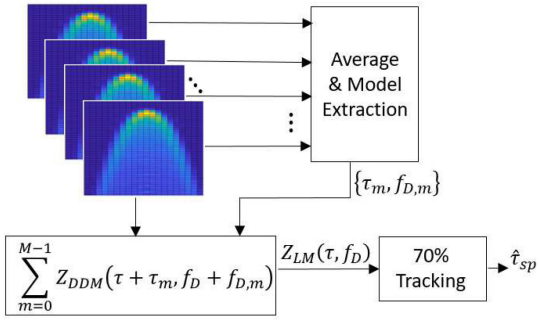

Fig. 4. MLM tracking block diagram.

When taking into account the complete signal, that is the K segments of length N, the solution is analogous to the noncoherent averaging of the DDM

$$Z_{\mathrm{LM}}(\tau, f) = \frac{1}{K}\sum_{k=0}^{K-1}(\mathbf{y}^k(\tau, f))^{\mathrm{H}}\boldsymbol{\chi}^{-1}\mathbf{y}^k(\tau, f). \tag{15}$$

This function can also be represented in the delay-Doppler plane and it is what we called LM in [6]. The delay value corresponding to its maximum is the MLE $\hat{\tau}_{sp}$.

A. LM Limitations in GNSS Ocean Altimetry

The LM is an alternative method to the DDM that uses a larger portion of the total reflected power through the combination of the complex cross-correlation results according to the signal model, taking into account the spreading due to the WAF. It is a preprocessing approach in the sense that it uses the raw signal samples to calculate the LM and also the best solution according to the MLE criteria. However, it does not present any improvement in the altimetry performance compared to the algorithms based on DDM observables, as we found out when using it with simulated signals and real raw data from TDS-1. This disappointing result can be understood due to the low SNR of the reflected signal. The estimation of the amplitude vector is performed implicitly in the calculation of the LM, as described in (15). The SNR levels of each complex cross-correlation result observed in real data from TDS-1 and CYGNSS are too low to make proper amplitude estimations, which in turn impacts the precision of the estimator $\hat{\tau}_{sp}$. Assuming the distribution in (10), the SNR needed to obtain an estimate through a 1 ms integration within a 10% error and 90% confidence is around 45 dB, which is 25 dB higher than the observed SNR values, depicted in Fig. 3. This means that even though the LM is the best solution in the MLE sense, its performance departs from the optimal [12] in this particular problem due to its low-signal power. However, some modifications of this algorithm can actually achieve a better performance.

Assuming that the separation of the delay-Doppler values of the contributions in the signal model are larger than the WAF spread, that is,

$$|\tau_m - \tau_l| \geq T_c \quad m, l = 0 \ldots M-1 \quad m \neq l \tag{16}$$

$$|f_m - f_l| \geq \frac{1}{T_i} \quad m, l = 0 \ldots M-1 \quad m \neq l \tag{17}$$

where T_c is the chip duration in the code signal and T_i the coherent integration time, the matrix $\boldsymbol{\chi}$ becomes an identity matrix of size $M \times M$. Thus, the LM can be obtained as follows:

$$\begin{aligned} Z_{\mathrm{LM}}(\tau, f) &= \frac{1}{K}\sum_{k=0}^{K-1}\sum_{m=0}^{M-1}|y^k(\tau+\tau_m, f+f_m)|^2 \\ &= \sum_{m=0}^{M-1} Z_{\mathrm{DDM}}(\tau+\tau_m, f+f_m). \end{aligned} \tag{18}$$

In this case, the LM becomes a postprocessing technique since it combines the DDM values instead of the complex cross-correlation results, and also it does not involve any matrix inversion as in the general solution in (15), which may lead to numerical issues in the estimation.

Following this idea, we defined MLM, the modified version of the LM that calculates each point of the map as described in (18) but using delay and Doppler intervals smaller than those specified in (16) and (17). This postprocessing approach is suboptimal according to the MLE solution since it ignores the deterministic correlation between the cross-correlation results that are closer than the WAF spreading. This simplified representation would lead to an inferior performance than the LM for high SNR ranges, i.e., if not restricted by the limitations described in Section III-A. However, for the observed SNR values, it performs better, since it uses the already averaged results rather than relying on the SNR of each individual cross-correlation value. Moreover, we obtained better precision when tracking the 70% of the peak value of the MLM, following the idea of p70, rather than tracking its maximum. The block diagram that represents the algorithm steps is depicted in Fig. 4. As shown in the first block, we used an average of consecutive DDMs to obtain the distribution of the reflected power in the delay-Doppler plane, which determines the set $\{\tau_m, f_m\}_{m=0\ldots M-1}$, instead of using the iso-delay and iso-Doppler lines.

IV. Performance Assessment

In order to characterize and compare the performance of the MLM with the DDM-based algorithms, we performed simulations using a Monte Carlo approach. We used the ZV model to obtain the DDM power distribution in the delay-Doppler plane and generated multiple realizations based on the SNR levels observed in the available experimental data. We took special care

in the statistical properties of the DDM, appropriately modeling the distribution and moments for each point in the map and the statistical correlation among them. The details of the simulation scenario and results are presented in the following sections.

A. Stochastic DDM Model

To generate DDM realizations, we followed the model in (6) considering a complex Gaussian amplitude vector, independent of the noise $\mathbf{v}^k$ term and uncorrelated between its elements (the phase and magnitude of two nonoverlapping cells α_m^k and α_l^k with $l \neq m$ are considered independent) and between different batches (the integration time perfectly matches the coherence time of the signal). Then, replacing (1) in (8), we can express the cross-correlation results in two terms, one purely corresponding to the signal $y_s^k(\tau, f)$ and another related to the thermal noise $y_v^k(\tau, f)$,

$$y^k(\tau, f) = y_s^k(\tau, f) + y_v^k(\tau, f). \tag{19}$$

Both complex terms are normally distributed with zero-mean, and constant variance in the case of the noise term, equal to σ_v^2 for every delay-Doppler pair (τ, f), and $\sigma_s^2(\tau, f)$ for the signal term which depends on the geometry, receiver specifications and the state of the ocean, as described in the ZV model.

The DDM value in (τ, f) is Chi-Squared distributed with 2 K degrees of freedom when normalizing by the variance of the averaged Gaussian terms

$$Z'_{\text{DDM}}(\tau, f) = \frac{2K Z_{\text{DDM}}(\tau, f)}{\sigma_v^2 + \sigma_s^2(\tau, f)} \sim \chi^2_{2K}. \tag{20}$$

The corresponding mean and variance are as follows:

$$\mathbb{E}\{Z_{\text{DDM}}(\tau, f)\} = \sigma_v^2 + \sigma_s^2(\tau, f) \tag{21}$$

$$\mathbb{V}\{Z_{\text{DDM}}(\tau, f)\} = \frac{\left(\sigma_v^2 + \sigma_s^2(\tau, f)\right)^2}{K} \tag{22}$$

which models both the speckle and thermal noise. Finally, for a proper modeling of the DDM, we included the correlation between different map points filtering independent realizations according to the structure given by the WAF.

With this statistical characterization, we can generate DDMs realizations for a given signal represented by its mean power $\sigma_s^2(\tau, f)$, which, as stated above, can be obtained with the ZV model or extracted experimentally from averaged DDMs and subtracting the noise floor. The noise variance σ_v^2 value depends on the desired SNR for the simulation. In this article, we used the SNR definition as in [1].

B. Simulation Results

We implemented the processing tasks described in Fig. 4 and applied it to a set of 5000 realizations for each SNR value considered. The signal power distribution in the delay-Doppler plane ($\sigma_s^2(\tau, f)$) was obtained using the ZV model with the CYGNSS geometry to generate the DDMs without noise. The algorithm averages 20 DDMs realizations to determine the delay-Doppler pairs of the first M highest values and make the signal model needed for the MLM. Then, the MLM is computed using (18) and the SP delay value is estimated by tracking the 70% of its maximum. The delay and Doppler resolution in the model is 0.25 chips and 500 Hz, respectively, the same as the original DDMs. We used sinc interpolation to perform the tracking with submeter delay resolution. The precision obtained for each SNR scenario is estimated through the computation of the standard deviation of the delay estimation. Fig. 5 depicts the precision values obtained for the observed SNR which shows a better performance with the MLM compared to p70. These results correspond to a moderate wind speed over the ocean of 6 m/s. The dependence of the method performance with this parameter is not explored in this article, however we do not expect much variation for values larger than 4 m/s and higher. Cases with weaker winds have a stronger coherent component, which is not considered in our signal model. The MLMs are obtained with a model size of $M = 20$, which spans 1.75 chips in the delay dimension and 2 kHz in Doppler. We tested multiple values and found the best results with sizes between 15 and 30 contributions. To quantify the improvement in performance, we used exponential curves fitted to the estimated results, also depicted in Fig. 5 and defined the SNR gain as the difference in SNR for which the MLM obtains the same precision as p70. Fig. 6 shows the gain curve obtained from the simulation. In these curve, we can see that the proposed method achieves the same performance as p70 with an SNR 1.64 to 3.66 dB lower, which impacts directly in the restrictions of the receiver sensitivity.

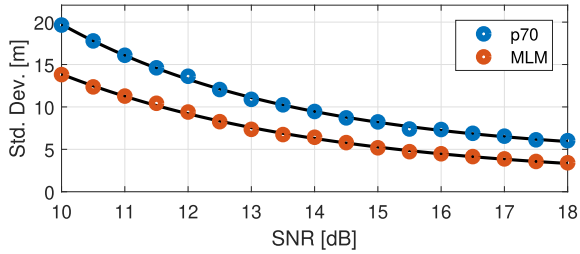

Fig. 5. Estimated precision with simulated DDMs.

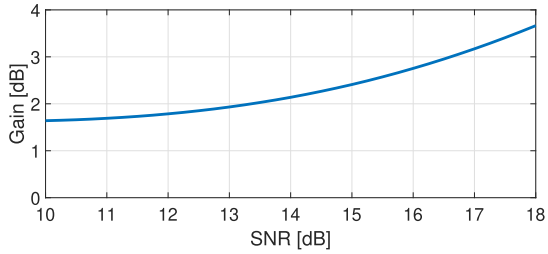

Fig. 6. Estimated SNR gain with simulated DDMs.

These results verify that the MLM exploits the reflected power in a more efficient way than the single point tracking methods by taking into account its distribution in the delay-Doppler plane, leading to a better precision in the delay estimation.

C. Test With CYGNSS DDMs

We also used a set of DDMs from CYGNSS to test the performance of the MLM with actual DDMs. Fig. 7 shows the coarse SP position as reported in the metadata of the 150 000 reflections used in the test. We confirmed some of the assumptions

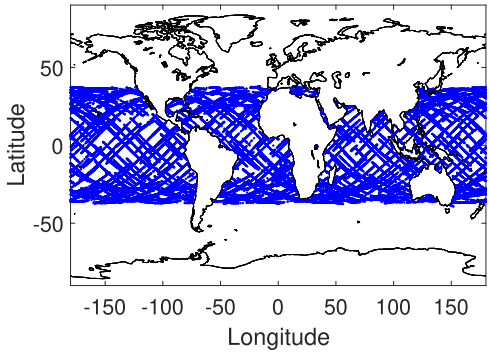

Fig. 7. SP position of the CYGNSS DDMs in the dataset.

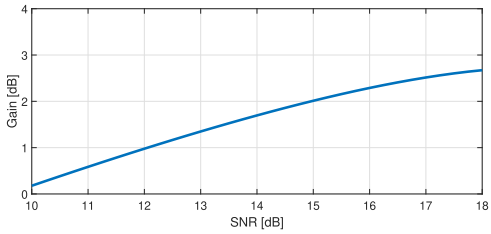

Fig. 8. Estimated SNR gain with CYGNSS DDMs.

in our model by estimating their statistical properties, such as the relation between its mean and variance expressed in (21) and (22), and the statistical correlation between map points. Although we obtained higher values in the standard deviation of the delay estimation for both methods, mainly because of issues with the data quality control, smaller sets in the averaging and imperfections in the detrending of the delay estimation, the results using the MLM showed a better performance compared to p70. The estimated gain is presented in Fig. 8. Even though it shows lower values than the simulated results, the method still gains 1.69 to 2.62 dB for SNR values between 14 to 18 dB, which are the most common values in the dataset, as shown in Fig. 3, confirming the potential of the proposed method. One of the main reasons, the results with CYGNSS DDMs differ from the simulated is that, the set of actual DDMs presents diverse conditions for each case regarding geometry, sea state, coherence in signal, among other characteristics, whereas the simulation results only contemplate variations due to the thermal and speckle noise for a given geometry and wind speed over the ocean in a completely diffuse regime.

V. Conclusion

We presented a performance analysis of the MLM method. It was first introduced as a formal derivation of the estimator for the SP delay value based on the MLE theory to improve the precision in code altimetry for ocean-reflected signals. Since the latter procedure is not suitable for the low-SNR signal levels found in practice, we proposed a modification of the LM that uses the already processed DDMs in a postprocessing manner to generate the MLM and track the 70% of its maximum. It employs an *a priori* model of the reflected signal power distribution in the delay-Doppler plane to calculate the estimates, which implies a more efficient use of the signal resources than the single tracking point methods. We estimated the precision in the delay estimation with a Monte Carlo approach using a complete statistical characterization of the DDMs. The results presented showed an improvement in the tracking performance using the MLM, with SNR gain values between 1.64 and 3.66 dB, increasing with the SNR.

In addition, we made a similar estimation using a dataset from the CYGNSS mission. The SNR-gain results, ranging between 1.69 and 2.62 dB for the most common received SNR, were lower than the expected theoretical values. However, they are still significant gains for an application that is severely constrained by the received signal power.

Future work includes an extension of the performance analysis for different geometries and state of the ocean to determine its impact in the estimation precision and optimal model size. Also, we will continue experimenting with actual data from space missions to make a more complete characterization of the method's performance in real scenarios.

References

[1] J. Mashburn, P. Axelrad, S. T. Lowe, and K. M. Larson, "Global ocean altimetry with GNSS reflections from TechDemoSat-1," *IEEE Trans. Geosci. Remote Sens.*, vol. 56, no. 7, pp. 4088–4097, Jul. 2018.

[2] C. Zuffada *et al.*, "Assessing the altimetric measurement from CYGNSS Data," in *Proc. IEEE Int. Geosci. Remote Sens. Symp.*, 2018, pp. 8292–8295.

[3] W. Li, E. Cardellach, F. Fabra, S. Rib, and A. Rius, "Assessment of spaceborne GNSS-R ocean altimetry performance using CYGNSS mission raw data," *IEEE Trans. Geosci. Remote Sens.*, vol. 58, no. 1, pp. 238–250, Jan. 2020.

[4] M. Unwin and P. Jales, "Mission description—GNSS reflectometry on TDS-1 with the SGR-ReSI," Surrey Satellite Technol. Ltd., Guildford, U.K., Tech. Rep., 2015.

[5] C. Ruf *et al.*, "The NASA EV-2 cyclone global navigation satellite system mission," in *Proc. IEEE Aerosp. Conf.*, 2013, pp. 1–7.

[6] S. Ozafrain, P. A. Roncagliolo, and C. H. Muravchik, "Maximum likelihood estimation for altimetry with ocean-reflected GNSS signals," in *Proc. 31st Int. Tech. Meeting Satellite Divis. Inst. Navig.*, 2018, pp. 2859–2868.

[7] V. U. Zavorotny and A. G. Voronovich, "Scattering of GPS signals from the ocean with wind remote sensing application," *IEEE Trans. Geosci. Remote Sens.*, vol. 38, no. 2, pp. 951–964, Mar. 2000.

[8] G. Giangregorio, M. D. Bisceglie, P. Addabbo, T. Beltramonte, S. D'Addio, and C. Galdi, "Stochastic modeling and simulation of delay doppler maps in GNSS-R over the ocean," *IEEE Trans. Geosci. Remote Sens.*, vol. 54, no. 4, pp. 2056–2069, Apr. 2016.

[9] M. Clarizia, C. Ruf, P. Jales, and C. Gommenginger, "Spaceborne GNSS-R minimum variance wind speed estimator," *IEEE Trans. Geosci. Remote Sens.*, vol. 52, no. 11, pp. 6829–6843, Nov. 2014.

[10] C. Chew, A. Colliander, R. Shah, C. Zuffada, and M. Burgin, "The sensitivity of ground-reflected GNSS signals to near-surface soil moisture, as recorded by spaceborne receivers," in *Proc. IEEE Int. Geosci. Remote Sens. Symp.*, Jul. 2017, pp. 2661–2663.

[11] Y. Wang and J. Morton, "Coherent reflections using closed-loop PLL processing of CYGNSS IF data," in *Proc. IGARSS IEEE Int. Geosci. Remote Sens. Symp.*, 2019, pp. 8737–8740.

[12] J. Ziv and M. Zakai, "Some lower bounds on signal parameter estimation," *IEEE Trans. Inf. Theory*, vol. 15, no. 3, pp. 386–391, May 1969.